Springer

KSME

Journal of Mechanical Science and Technology 24 (10) (2010) 1997~2006
www.springerlink.com/content/1738-494x
DOI 10.1007/s12206-010-0618-7

Numerical and experimental investigation of vortex breaker effectiveness on the improvement in launch vehicle ballistic parameters

Mahdi N. Mahyari[1,*], Hasan Karimi[2], Hasan Naseh[2] and Mehran Mirshams[2]

[1]*Faculty of Mechanical Engineering, K.N Toosi University of Technology, Tehran, Iran*
[2]*Faculty of Aerospace Engineering, K.N Toosi University of Technology, Tehran, Iran*

(Manuscript Received July 1, 2009; Revised April 22, 2010; Accepted May 9, 2010)

Abstract

The focus of the present study is to investigate the effectiveness of installing vortex breakers at the outlet of launch vehicle tanks on postponing vortex formation and decreasing the critical height of propellants while discharging. Analytical results in the absence of a vortex breaker show that the effects of the Weber and Reynolds numbers in the flow field can be ignored for values greater than 720 and 1.1×10^5, respectively; and critical height can be considered as a function of Froude number under aforementioned conditions. The analytical criteria are verified by two-dimensional, axis symmetrical, transient and two-phase numerical model. Eventually, some experiments are conducted to examine the effectiveness of the applied vortex breakers in reduction of the critical height of propellant. Experimental results show that a 30% decrease can be achieved in critical height by using a particular type of vortex breaker. Additionally, the carried out simulations for an existing two-stage launch vehicle indicate a 13% increase in orbital altitude, which in turn proves the considerable improvement in launch vehicle mass/energetic capabilities.

Keywords: Critical height; Launch vehicle; Propellant; Vortex breaker; Weber and Reynolds numbers

1. Introduction

Generally, vortex flow formation at the outlet of a tank is a significant and undesirable phenomenon. Vortex formation in flux fields with either free surface or near a sink (in several systems such as water supply systems or liquid propellant tanks of launch vehicles) is of great importance. As the tank draining nears the end, some free surface disturbances may occur as shown in Fig. 1(a). The height of the liquid in this condition is called the dimple height. As discharge continues, the dimple extends rapidly toward the outlet and forms a swirling air funnel. This leads to the penetration of gas in the outflowing liquid as depicted in Fig. 1(b). The height of the liquid when the tip of the funnel reaches to the outlet is called the critical height.

Gas presence in the expulsion liquid causes a sudden increase in the turbo-pump rotational velocity and combustion instability in the launch vehicle engine. Since feed pump operation is not recommended in such conditions, the engine must be stopped before any gas ingestion occurs. A common approach to resolve this problem is to consider the overcharging of the propellant tanks followed by an adequate discharge until the propellant height reaches the critical value. However, the overcharged propellant will remain in the tank at the end of the mission. It is obvious that the excess propellant lowers the ballistic characteristics of a launch vehicle such as orbital altitude and velocity. Applying a vortex breaker at the bottom of a tank reduces the volume of the remaining propellant. Vortex breakers postpone the time of vortex formation by diminishing the swirling flow and changing the pressure and velocity fields near the outlet.

Some analytical and experimental studies have been performed on vortical flows in hydraulic engineering, in the past. In some cases the free surface is located too close to the outlet, as is done in a power plant's intake [1, 2]. A simple device was suggested for preventing vortex formation in a small scale cylindrical container by L. Gowda et al. [3, 4]. The effects of the initial tangential velocity and the intake eccentricity on the critical height were examined by Piva et al. [5]. Also, an unsteady three-dimensional numerical model was created by the European Space Agency (ESA) in order to simulate the flow field near the vortex breaker in the oxidizer tank of the ARIANE 5 launcher [6] (see Fig. 2). On the other hand, to date no research has been carried out to examine the effect of applying a vortex breaker on the launch vehicle mass-energetic capabilities. Therefore, the main aim of this paper is

† This paper was recommended for publication in revised form by Associate Editor Do Hyung Lee
* Corresponding author. Tel.: +989126487870, Fax: +982177791045
E-mail address: mahyari@sina.kntu.ac.ir

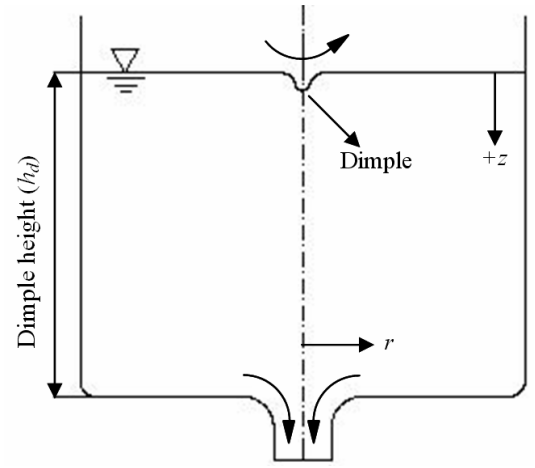

(a)

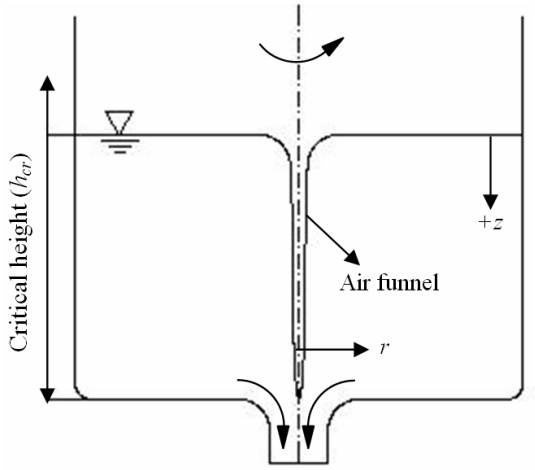

(b)

Fig. 1. Geometry of a tank near the outlet. (a) Formation of a dimple on the surface. (b) The dimple extends and forms an air funnel.

to examine the effect of using vortex breakers on the improvement of ballistic parameters of a launch vehicle.

The attempts by the launch vehicle community for attaining an appropriate design by using the existing technologies and instruments have led to successful results, for instance see [7-9]. In this research, it is suggested that the optimization of the design parameters is incorporated in the conceptual design process by which the reduction of propellant and structure mass can be achieved. This, in turn, leads to the improvement in the ballistic characteristics. To this end, the amount of reduction in critical height is calculated experimentally, which leads to a decrease in fuel and oxidizer mass. Then, the achieved mass reduction is utilized in the performance simulation algorithm and thereby the enhancement of the capabilities of launch vehicle is illustrated.

Launch Vehicle Conceptual Design (LVCD) code was applied to illustrate the effect of vortex breakers on improvement in launch vehicle performance [10]. In the LVCD software, the results of various researches are employed to develop a

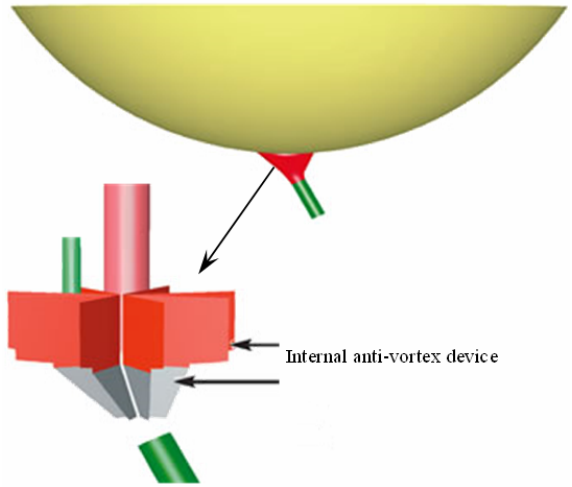

Fig. 2. The geometry of liquid oxygen tank bottom of ARIANE 5 with internal anti-vortex device [6].

conceptual design algorithm for launch vehicle design [9, 11, 12]. Consequently, a launch vehicle with optimized major design parameters would be the outcome of this developed algorithm. Finally, the improvements in orbital altitude and velocity of a two-stage launch vehicle are evaluated by this code.

2. Dimensional analysis

For the purposes of the present study, let the critical height be defined as the submergence of the outlet at which incipient air entrainment is possible. Considering the critical height as the dependent variable, the following functional relationship may be written as

$$h_{cr} = f_1(d, D, \mu, \rho, \sigma, \upsilon, g) \tag{1}$$

By choosing d, ρ and υ as the repeating variables and doing dimensional analysis of the variables of Eq. (1), the following is obtained.

$$\frac{h_{cr}}{d} = f_2\left(\frac{D}{d}, \frac{\rho \upsilon d}{\mu}, \frac{\upsilon}{\sqrt{gd}}, \frac{\rho \upsilon^2 d}{\sigma}\right) \tag{2}$$

Since the parameter D/d is large enough in the tests, the effect of the boundary of the tank on the vortex formation is negligible and can be dropped from Eq. (2), i.e.

$$\frac{h_{cr}}{d} = f_3(\mathrm{Re}, Fr, We) \tag{3}$$

It is necessary to find ranges for the dimensionless parameters in Eq. (3) that h_{cr}/d is not a strong function of these parameters. This goal can be obtained analytically to reduce the number of test iterations [13-17].

3. Analytical consideration

The considered flow situation has been depicted in Fig. 1. Since in the vicinity of the vertical axis the flow is assumed steady, axis-symmetric and laminar, the equations of motion for an incompressible fluid are as follows:

$$\frac{1}{r}\frac{\partial}{\partial r}(r v_r)+\frac{\partial v_z}{\partial z}=0 \tag{4}$$

$$v_r\frac{\partial v_r}{\partial r}+v_z\frac{\partial v_r}{\partial z}-\frac{v_\theta^2}{r}= =-\frac{1}{\rho}\frac{\partial P}{\partial r}+\nu\left(\frac{\partial^2 v_r}{\partial r^2}+\frac{1}{r}\frac{\partial v_r}{\partial r}-\frac{v_r}{r^2}+\frac{\partial^2 v_r}{\partial z^2}\right) \tag{5}$$

$$v_r\frac{\partial v_\theta}{\partial r}+v_z\frac{\partial v_\theta}{\partial z}+\frac{v_r v_\theta}{r}= =\nu\left(\frac{\partial^2 v_\theta}{\partial r^2}+\frac{1}{r}\frac{\partial v_\theta}{\partial r}-\frac{v_\theta}{r^2}+\frac{\partial^2 v_\theta}{\partial z^2}\right) \tag{6}$$

$$v_r\frac{\partial v_z}{\partial r}+v_z\frac{\partial v_z}{\partial z}= =-\frac{1}{\rho}\frac{\partial P}{\partial z}+\nu\left(\frac{\partial^2 v_z}{\partial r^2}+\frac{1}{r}\frac{\partial v_z}{\partial r}+\frac{\partial^2 v_z}{\partial z^2}\right)+g \tag{7}$$

The model is obtained by superimposing a radial flow on a free vortex flow given by

$$v_\theta=\frac{\Gamma_\infty}{2\pi r}f(r) \tag{8}$$

Γ_∞ is the value of circulation in free vortex flow where the radius is far enough from the axis. Near the pipe entrance where $r<r_\circ$ and $z\le h_{cr}$, the radial velocity can be approximately assumed as $-a r$ [1]. By using this assumption, from the Eq. (4) the axial velocity is obtained as $2az$. Since the axial velocity is equal to υ at $z=h_{cr}$, then a can be calculated by $\upsilon/2h_{cr}$. Substituting Eq. (8) into Eq. (6) yields:

$$v_r\frac{f'}{r}+\nu\frac{d}{dr}\left(\frac{f'}{r}\right)=0 \tag{9}$$

Note that $v_r=-ar$, $f\to 1$ for $r\to\infty$, and v_θ has no singularity at $r=0$. Then, by substituting the solution of the Eq. (9) into Eq. (8), a tangential velocity distribution is obtained as follows.

$$v_\theta=\frac{\Gamma_\infty}{2\pi r}\left[1-\exp\left(-\frac{1}{2}\frac{a}{\nu}r^2\right)\right] \tag{10}$$

The maximum tangential velocity ($v_{\theta,c}$) occurs at the distance r_c. This distance is measured from the axis and is given by

$$r_c^2=2.5\frac{\nu}{a} \tag{11}$$

Therefore, the maximum value of tangential velocity is given by

$$v_{\theta,c}^2=0.00516\,\Gamma_\infty^2\frac{a}{\nu} \tag{12}$$

Eq. (10) can be normalized by Eqs. (11) and (12) as follows:

$$\frac{v_\theta}{v_{\theta,c}}=1.4\frac{r_c}{r}\left[1-\exp\left(-1.25\left(\frac{r}{r_c}\right)^2\right)\right] \tag{13}$$

The critical height is obtained from the pressure distribution and by substituting Eq. (10) into Eqs. (5) and (7). Then integrating on the resulting equation leads to

$$P=P_\circ+\int_0^r\rho\frac{v_\theta^2}{r}dr-\frac{1}{2}\rho a^2 r^2 \tag{14}$$

Where $P_\circ$, the pressure at the tip of vortex due to surface tension, is equal to $-2\sigma/r_c$. For distances beyond r_c, P tends to hydraulic pressure. The third term on the right side of Eq. (14) is small compared to the second term for $r<r_\circ$. Integrating from axis to $r=r_\circ$ and by using Eqs. (13) and (14), the following equation is obtained.

$$h_{cr}=-\frac{2\sigma}{r_c\rho g}+3.4\left[1-0.5\left(\frac{r_c}{r_\circ}\right)^2\right]\frac{v_{\theta,c}^2}{2g} \tag{15}$$

Where r_c is given by Eq. (11). The radius ratio in Eq. (15) can be replaced by $5\nu h_{cr}/\left(\upsilon r_\circ^2\right)$. This value is small enough so that the value of bracket in Eq. (15) can be assumed to be unity. Considering Eqs. (11) and (12), Eq. (15) is simplified as follows.

$$h_{cr}^2=-0.9\frac{\sigma}{\rho g}\sqrt{\frac{\upsilon h_{cr}}{\nu}}+0.0043\frac{\Gamma_\infty^2\upsilon}{g\nu} \tag{16}$$

In terms of dimensionless parameters, Eq. (16) can be rewritten as the following form.

$$\left(\frac{h_{cr}}{d}\right)^2=-0.89\,Fr^2\,\mathrm{Re}^{1/2}\left(\frac{h_{cr}}{d}\right)^{1/2}We^{-1}+ +0.0026\,Fr^2\,\mathrm{Re}\,N_\Gamma^2 \tag{17}$$

A criterion for neglecting effects of surface tension may be established by requiring that ratio between the surface tension and circulation terms in Eq. (15) to be less than 10%. Thus

$$\frac{\rho v_{\theta,c}^2 r_c}{\sigma}>12 \tag{18}$$

Substituting Eqs. (11) and (12) into Eq. (18) leads to the following equation.

$$We > 720\, Fr^{1/2}\, N_{\Gamma}^{-3/2}\, \mathrm{Re}^{-1/4} \tag{19}$$

The values of $Fr^{1/2}$, $N_{\Gamma}^{3/2}$ and $Re^{1/4}$ for conditions of a typical model are of the order of 1, 0.1 and 10, respectively. Therefore, the criterion for neglecting the surface tension will be $We > 720$. Moreover, a criterion for neglecting the effect of viscosity can be established by requiring that turbulent viscosity be greater than 5ν. This condition has less than a 10% effect on the critical height [18]. It follows from Eq. (16) that without the surface tension term, this criterion is met when the following condition is satisfied.

$$\mathrm{Re} > 1.1\times 10^{3}\left(\frac{h_{cr}}{d}\right)^{2}\frac{gd^{3}}{\Gamma_{\infty}^{2}} \tag{20}$$

The value of $(h_{cr}/d)(\sqrt{gd^{3}}/\Gamma_{\infty})$ is of the order of 10, and the criterion for neglecting viscous effects is $\mathrm{Re} > 1.1\times 10^{5}$. Under the conditions where $\mathrm{Re} > 1.1\times 10^{5}$ and $\mathrm{We} > 720$, Eq. (17) can be simplified as follows:

$$\frac{h_{cr}}{d} = 1.55\, Fr^{1/3} \tag{21}$$

Eq. (21) is the main goal of this section. This relation implies the critical height of propellants can just be assumed as a function of Froude number provided that $\mathrm{Re} > 1.1\times 10^{5}$ and $\mathrm{We} > 720$. In other words, neglecting the viscous and surface tension effects of the flow, the number of the required tests can be decreased significantly.

4. Numerical investigation

Generally, the vortex formation at the propellant tanks outlet is a 3-D, unsteady, turbulent and two-phase phenomenon. Thus, a complete numerical solution is time-consuming and expensive. Instead, a 2-D, axis-symmetric, transient and two-phase numerical model is established so as to simulate the flow field. Both Reynolds and Weber numbers are greater than the criteria mentioned in section (3). According to Eq. (21), the Froude number is the most important parameter which affects the critical height when $\mathrm{Re} > 1.1\times 10^{5}$ and $\mathrm{We} > 720$. Under these conditions, the numerical model should be carried out for various Froude numbers to show the variation of the critical height.

The domain of the solution, a structured mesh, and the boundary conditions are shown in Fig. 3. Air enters the inlet boundary with constant pressure and water is expulsed with constant mass flow rate at the outlet. Solution continues while the volume fraction of water at the outlet is equal to 1. Passing the air bubble through the outlet reduces the water volume fraction. Therefore, the boundary condition at the outlet will not be satisfied and solution will be stopped. The boundary

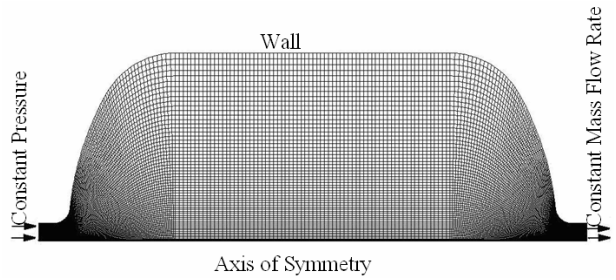

Fig. 3. The geometry of tank with 30040 structured elements. Boundary conditions can be supposed constant pressure at inlet and constant mass flow rate at outlet.

condition for the axis of symmetry can be expressed as $(\partial\varphi/\partial r)_{r=0}=0$, Where φ represents any arbitrary physical quantity like velocity components or pressure.

The tracking of the interface between the phases is accomplished by the solution of a continuity equation for the volume fraction of different phases. For the ith phase, this equation has the following form [19]:

$$\frac{\partial\alpha_i}{\partial t} + \vec{V}.\nabla\alpha_i = 0 \quad , \quad \sum_{i=1}^{2}\alpha_i = 1 \tag{22}$$

A single set of momentum equations is solved throughout the domain, and the resulting velocity field is shared among the phases. The momentum equations depend on the volume fractions of all phases through the properties ρ and μ [19].

$$\begin{aligned}\frac{\partial\left(\rho\vec{V}\right)}{\partial t} + \nabla.\left(\rho\vec{V}\vec{V}\right) = \\ = -\nabla P + \nabla.\left[\mu\left(\nabla\vec{V} + \nabla\vec{V}^{T}\right)\right] + \rho\vec{g} + \vec{F}\end{aligned} \tag{23}$$

In general, for an n-phase system, the volume-fraction-averaged φ (like density or viscosity) takes the following form [19]:

$$\varphi = \sum_{i=1}^{n}\alpha_i\varphi_i \tag{24}$$

By using a 2-D axis-symmetric model, the critical height of the fluid can be estimated as a function of Froude number under the conditions mentioned for Eq. (21). But investigation of the effects of the vortex breakers requires a fully 3-D numerical model. However, it is possible to show the effect of a circular plate located at the top of the intake on the flow field using a two dimensional axis-symmetric model. Fig. 4 shows a part of the unstructured mesh generated for this object.

The $k-\varepsilon$ model was employed to simulate the turbulence in numerical code. A segregated solver was used to solve the flow field equations, and the transient SIMPLE algorithm was applied to couple the pressure and velocity fields. Also, convection terms of governing equations were made discrete using the first-order method. In this numerical model, character-

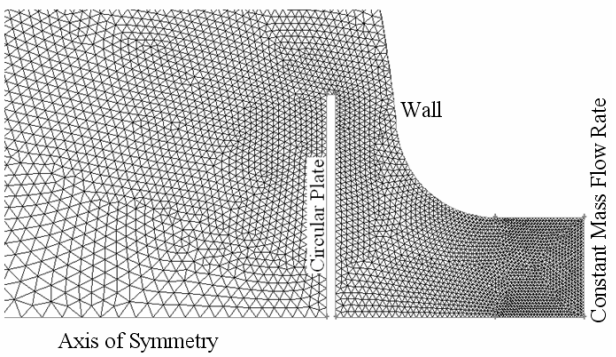

Fig. 4. The geometry of tank with 23095 unstructured elements considering a circular plate near the outlet.

istic time is a function of the free surface velocity and the representative length of the free surface elements. The Courant number is a dimensionless parameter which compares the time step in a calculation to the characteristic time of transit of a fluid element across a control volume:

$$\Delta t = CFL \times \Delta t_{characteristic} = CFL \times \frac{\Delta x_{cell}}{v_{free\,surface}} \tag{25}$$

Where CFL is Courant number, Δx_{cell} is representative length of free surface elements and $v_{free\,surface}$ is free surface velocity. Generally, the Courant number is chosen as 0.25 in 2-D problems [20]. Therefore, the order of the time step can be calculated by dividing the order of representative length of interface elements by the order of the free surface velocity as the following:

$$O(\Delta t) = CFL \frac{O(\Delta x_{cell})}{O(v_{free\,surface})} = \\ = 0.25 \frac{1 \times 10^{-3}(m)}{1(m/\sec)} = 2.5 \times 10^{-4} \sec. \tag{26}$$

According to Eq. (26), the time step can be chosen equal to 2.5×10^{-4} second in the solution. However, to enhance the accuracy, the time step was considered to be 1.0×10^{-4} second.

Fig. 5 shows contours of velocity magnitude for both the gas and the liquid phases. The contours of the tangential velocity are illustrated in Fig. 6. It can be seen that the tangential velocity of a particle increases while it is moving towards the outlet. Fig. 7 shows the stages of air funnel formation at the interface of phases and the penetration of air towards the outlet. Figs. 8-10 demonstrate contours of velocity magnitude, tangential velocity and phases, respectively, but for the case where a circular plate has been located on top of the intake (see Fig. 4). Comparing Fig. 6 with Fig. 9 shows that tangential velocity decreases effectively by means of a flat plate. Also, it can be seen that an air funnel does not appear at the axis of the tank where maximum axial velocity occurs (Fig. 10). These two phenomena reduce the critical height by postponing vortex formation and diminishing swirling flow.

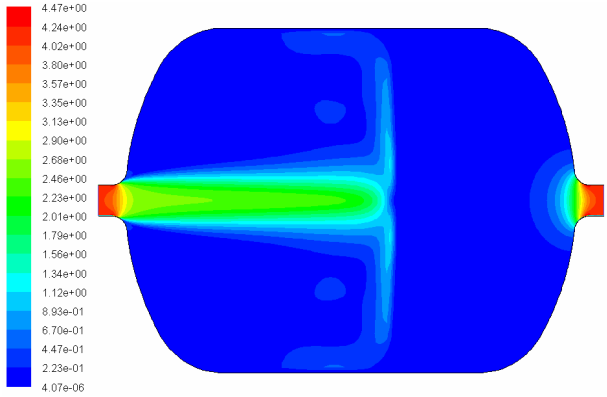

Fig. 5. Contours of velocity magnitude.

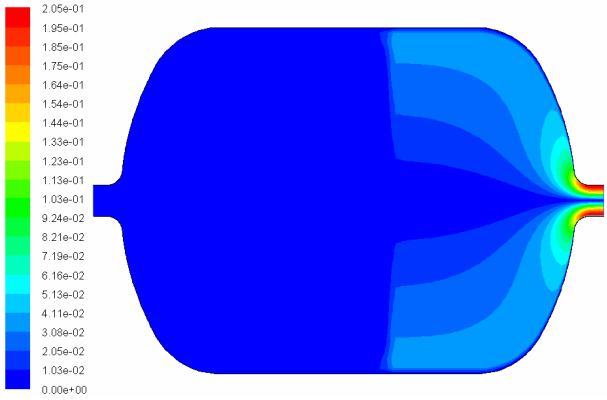

Fig. 6. Contours of tangential velocity.

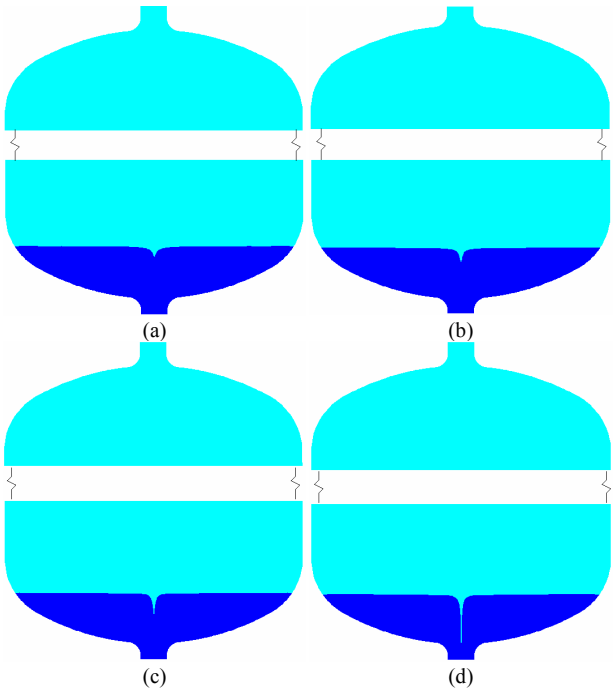

Fig. 7. The stages of vortex formation and penetration of air towards the intake.

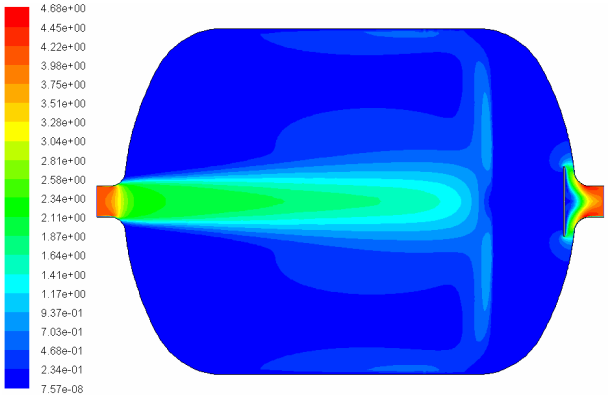

Fig. 8. Effect of a circular plate on velocity magnitude.

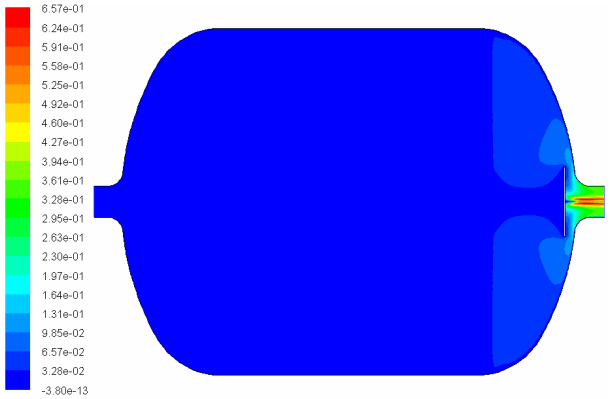

Fig. 9. Effect of a circular plate on tangential velocity.

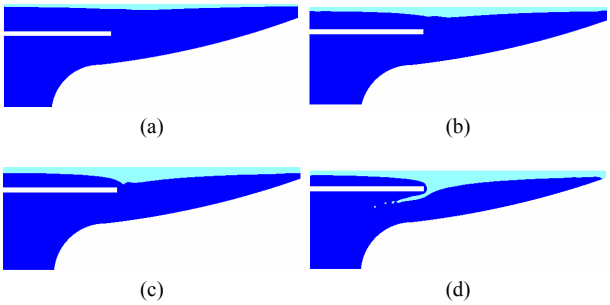

Fig. 10. Effect of a flat plate on interface disturbance and reduction in critical height during the time.

To verify whether the effect of the viscosity on the critical height is negligible for Reynolds number greater than 1.1×10^5, the variation of the critical height was compared when Reynolds number varies from 4.5×10^5 to 9.0×10^5 at a constant Froude Number ($Fr = 3.882$). As represented in Table 1, numerical results show just 5.6% difference in critical height when Reynolds number becomes twice.

Also, mesh independency of the numerical solution was examined by comparing the results of a coarse mesh with a finer mesh. The differences in Table 2 show that the mesh used in the model is fine enough.

Fig. 11 shows that the numerical results are in good agreement with the analytical result (Eq. (13)) to estimate the variation of tangential velocity. Since the effect of the wall shear stress was ignored for deriving Eq. (13), some deviation can be seen from the numerical results near the wall, especially for $r/r_c > 13$.

Table 1. Independency of Reynolds number for critical height at Fr = 3.882.

Outlet Geometry	Reynolds Number		Difference
	$Re = 4.5\times10^5$	$Re = 9.0\times10^5$	
Without plate (Fig. 4)	1.83	1.95	5.6%
With plate (Fig. 5)	1.04	1.07	2.8%

Table 2. Independency of mesh size for critical height at Fr = 3.882.

Outlet Geometry	Number of elements in mesh		Difference
	20×10^3	30×10^3	
Without plate (Fig. 4)	1.84	1.83	0.72%
With plate (Fig. 5)	1.07	1.04	2.6%

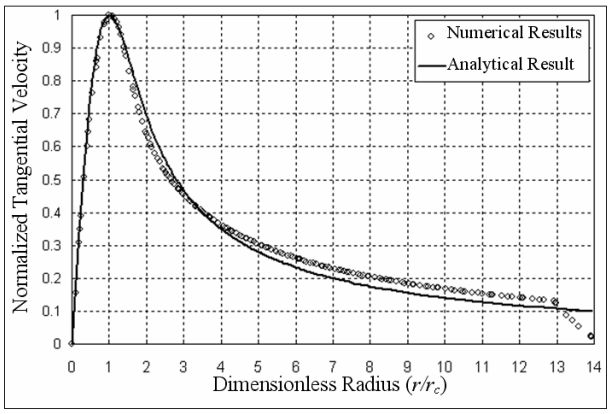

Fig. 11. The comparison of the analytical and numerical results for the tangential velocity variation.

5. Experiments

Some experiments are conducted to measure the dimple height in propellant tanks by applying different vortex breakers. This is because the values of Reynolds and Weber numbers for both the model and the prototype conditions are greater than the mentioned criteria (see Table 3). Thus, the experiments are dedicated to investigating the effects of Froude number on the dimple height for various outlets. In other words, the Froude number is a parameter which can relate the ratio of the inertia force to gravity force in flight conditions. Under flight conditions, the Froude number must be defined as a function of the axial acceleration (a_x), the pitch angle (θ) – the angle between launch vehicle axis and local horizon, – and local gravity (g) which is described below.

Table 3. The characteristic parameters for the under study two-stage launch vehicle.

Parameter	unit	1st stage of launch vehicle		2nd stage launch vehicle	
		Fuel (Kerosene)	Oxidizer (AK27*)	Fuel (UDMH**)	Oxidizer (N_2O_4)
ρ	kg/m^3	805	1603	795	1458
$\mu\times10^4$	$kg/m.s$	8.24	19	5.6	4.2
$\sigma\times10^3$	N/m	54	-	24.1	25.1
$\dot{m}$	kg/s	31.1	109	5.3	7.6
υ	m/s	3.92	6.93	6.16	4.86
a_x	m/s^2	55		65	
θ	deg	25		0	
Fr	-	1.52	2.69	3.97	3.13
$\mathrm{Re}\times10^{-5}$	-	4.3	6.6	3.2	6.2
$We\times10^{-4}$	-	5.2	-	4.6	5.1

* AK27: 73% HNO_3 + 27% H_2O
** UDMH: Unsymmetrical Di-Methyl Hydrazine

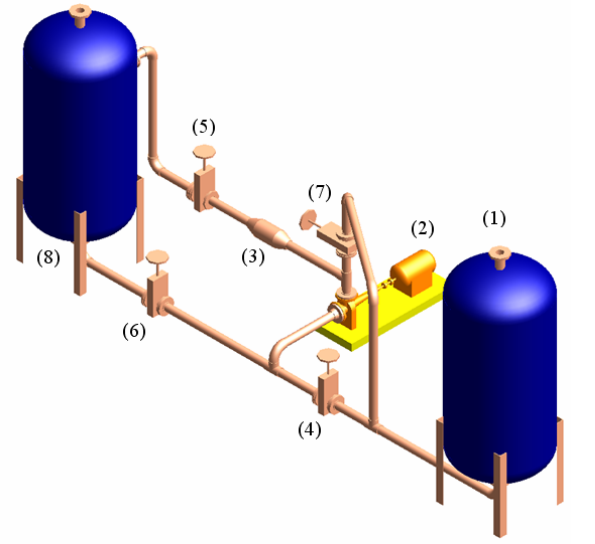

Fig. 12. Experimental setup: (1) propellant tank, (2) centrifugal pump, (3) magnetic flow meter, (4, 5, 6 &7) butterfly valves, (8) reservoir tank.

$$Fr = \frac{\upsilon}{\sqrt{(a_x + g\sin\theta)d}} \tag{27}$$

Eq. (27) can be simplified to $\upsilon/\sqrt{gd}$ when both a_x and θ are equal to zero. The tests are carried out using a transparent cylindrical tank made of Plexiglas with a diameter of 1.25 m and a height of 2.0 m with a drain hole of internal diameter 112 mm centrally located at the bottom of tank along the vertical axis (see Fig. 12). The working liquid in the experiments is water at room temperature. The pump discharges the water in the propellant tank to the reservoir tank while valves (4) and (5) are open and valves (6) and (7) are closed. The dimple height is measured for various flow rates and different vortex breakers. By changing the status of valves (4, 5 closed and 6, 7 open), the propellant tank can be recharged.

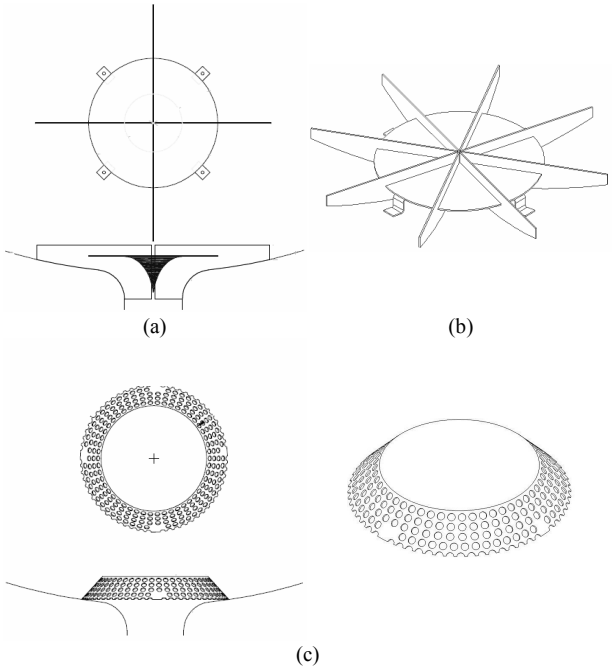

Fig. 13. Three types of vortex breaker.

The effects of four below devices are examined as vortex breakers, experimentally.

1. A circular flat plate with the diameter of $3d$.
2. A circular flat plate with the diameter of $3d$ with four radial blades (Fig. 13(a)).
3. A circular flat plate with the diameter of $3d$ with eight radial blades (Fig. 13(b)).
4. A circular flat plate with a porous wall (Fig. 13(c)).

The vortex breakers are installed at a height of 0.25d from the bottom of the tank. Increasing the installation height of the vortex breakers reduces its effectiveness. A vortex breaker with a diameter of 3d installed at a height of 0.25d provides a good balance between pressure drop and effectiveness [21]. Plate with diameter greater than 3d or installation height less than 0.25d leads to higher pressure drop and cavitation probability.

The variations of the dimensionless dimple height versus Froude number for the four cases are demonstrated in Fig. 14. The results show 11% decrease in the dimple height via installation of a flat plate with a diameter of $3d$ at the vicinity of intake. Also, by adding four radial blades to the flat plate, 18.5% decrease in the dimple height is noticed. Results show that a circular flat plate with a porous wall (Fig. 13(c)) is more effective and 30% reduction can be obtained in the dimple height and propellant weight (includes fuel and oxidizer weight for two stages of launch vehicle) will be reduced by 280 kg.

6. LVCD software definition

Launch Vehicle Conceptual Design (LVCD) software was

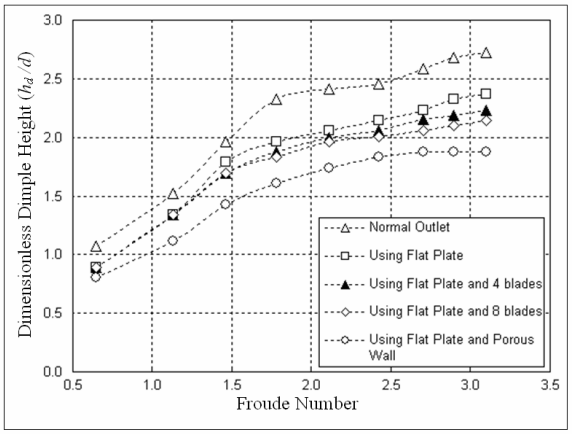

Fig. 14. The effects of different vortex breakers on the dimple height.

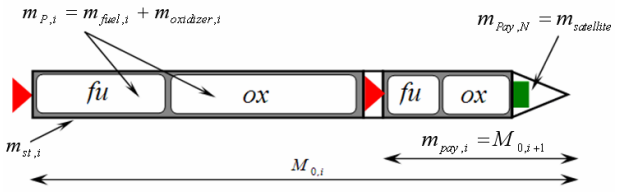

Fig. 15. Stage and block mass breakdown concept.

employed to illustrate the improvement in performance of a launch vehicle through the used vortex breaker. The main objectives of this software are a reduction of the cost and time of conceptual design phase. To this end, in this code, the weight of structure, the calculations of propellant and mass distribution of each stage, to launch maximum payload mass to the orbit, and the pitch program trajectory, to achieve the maximum final velocity, will be optimized [11].

Generally, in LVCD software, the calculations are performed based on optimization, but herein just a brief review of the most fundamental equations is presented to demonstrate and clarify how the variables change.

Let us assume that launch vehicle mass breakdown for ith stage is as follows (see Fig. 15):

$$M_{0,i} = m_{st,i} + m_{P,i} + m_{gua,i} + m_{Pay,i};\ i = 1,2,..,\mathrm{N} \tag{28}$$

Where N indicates the number of launch vehicle stages and is equal to 2 in this study. In addition, the characteristic velocity achieved at the end of ith stage is [22]:

$$V_i = -g.\, I_{sp,i}.\mathrm{Ln}\mu_{F,i};\ \mu_{F,i} = \frac{M_{0,i+1} + m_{st,i}}{M_{0,i}} \tag{29}$$

Where $\mu_{F,i}$ denotes the ratio of the final mass to the initial mass which is decreased by employing a vortex breaker. Also, $I_{sp,i}$ is called the specific impulse of the launch vehicle engine and is obtained through dividing the launch vehicle engine thrust to the exhaust mass flow rate.

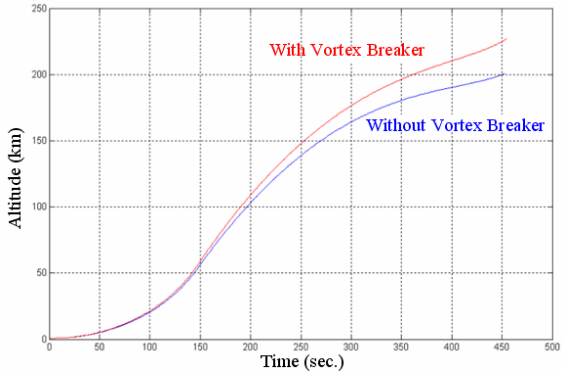

Fig. 16. Improvement in orbital altitude.

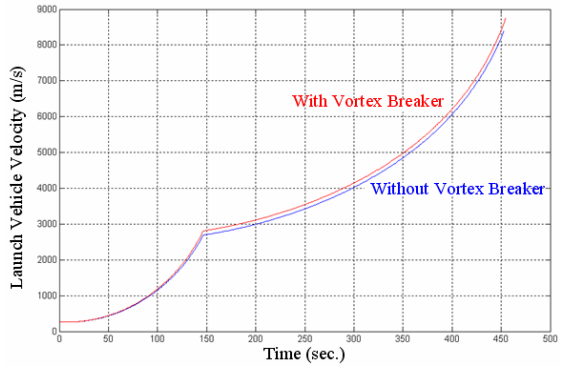

Fig. 17. Improvement in launch vehicle velocity.

7. Improvement in launch vehicle parameters

The ultimate goal of this effort is to simulate and improve the performance of a two-stage launch vehicle. The results of current simulation carried out by LVCD code for conditions, represented in Table 3, are in Figs. 16 and 17. The simulation results show that use of anti-vortex devices at the outlet of liquid-propellant tanks leads to enhancement in engine burning time, thrust-to-weight ratio, axial acceleration (especially in upper stages), and velocity and orbital altitude. Figs. 16 and 17 show, respectively, the improvement in orbital altitude and axial velocity achieved by means of a vortex breaker. Fig. 17 shows a 13% increase in the orbital altitude by using a specific type of vortex breaker (Fig. 13(c)) for the present two-stage launch vehicle.

8. Conclusions

Analytical investigation of this study indicates that viscous and surface effects of free-surface vortices can be neglected when the intake Reynolds and Weber numbers are greater than 1.1×10^5 and 720, respectively. Comparing the results of numerical simulation for Re = 4.5×10^5 with 9.0×10^5 reveals a maximum of 5.6% difference in critical height estimation at a constant Froude number, which in turn verifies the analytical criteria. So, in the experiments, the dimple height of the fluid was considered as a function of Froude number and outlet type. It is possible to achieve a 30% decrease by using a flat

plate with porous wall. In this case, the mass of the two-stage launch vehicle may be reduced by 280 kg and the result of LVCD simulation shows a 13% increase in the orbital altitude. This tacitly means that for a specific desired mission, with the specified orbital altitude, by decreasing the remaining mass, it is possible to carry a heavier payload mass to the same altitude.

Acknowledgment

The authors would like to express their deep gratitude to Dr. Kh. Alipour, Dr. M. Mohseni and A. Kalabkhani for their support and helpful comments.

Nomenclature

a : Factor of proportionality
a_x : Axial acceleration of launch vehicle at the end of each stage
CFL : Courant number
d : Inner diameter of intake pipe
D : Diameter of tank
f : Function
$\vec{F}$: Body force vector
Fr : Froude number
g : Local gravitational acceleration
h_{cr} : Critical height
$I_{sp,i}$: Specific impulse of ith stage
$\dot{m}$: Propellant mass flow rate
$M_{0,i}$: Total mass of ith stage
$m_{st,i}$: Dry structure mass of ith stage
$m_{P,i}$: Propellant mass of ith stage
$m_{gua,i}$: Guarantee (remaining) mass of ith propellant
$m_{Pay,i}$: Payload mass of ith stage
N : Number of launch vehicle stages
N_Γ : Circulation number
P : Pressure
$P_\circ$: Pressure at the tip of the vortex
r,θ,z : Radial, tangential and axial coordinates
r_c : Radial distance of maximum tangential velocity
$r_\circ$: Intake pipe radius
Re : Reynolds number
t : Time
υ : Mean velocity at the tank outlet
$v_{free\,surface}$: Free surface velocity
v_r, v_θ, v_z : Radial, tangential and axial component of velocity
$v_{\theta,c}$: Maximum tangential velocity
$\vec{V}$: Velocity vector
V_i : Launch vehicle velocity at the end of ith stage
We : Weber number
α_i : Volume fraction of ith phase in each cell
Δx_{cell} : Representative length of free surface elements
φ : Volume-fraction averaged of any physical quantity
φ_i : Volume fraction of ith phase
Γ_∞ : Circulation at the far field
ν : Kinematic viscosity
θ : Pitch angle of launch vehicle at the end of each stage
ρ : Density
σ : Surface tension of liquid

References

[1] J. E. Hite and W. C. Walter, Velocity of Air Core Vortices at Hydraulic Intakes, *Journal of Hydraulic Engineering*, 120 (3) (1994) 284-297.

[2] M. Maleewong, J. Asavanant and R. Grimshaw, Free Surface Flow under Gravity and Surface Tension Due to an Applied Pressure Distribution: I Bond Number Greater Than One-Third, *Journal of Computational Fluid Dynamic*, 19 (4) (2005) 237-252.

[3] B. H. Lakshamana Gowda, Draining of Liquid from Tanks of Square or Rectangular Cross Sections, *Journal of Spacecraft*, 33 (2) (1995) 311-312.

[4] S. Mizuki, B. H. Lakshamana Gowda and T. Uchibaba, Visualization Studies using PIV in a Cylindrical Tank with and without Vortex Suppressor, *Journal of Visualization*, 6 (4) (2003) 337-342.

[5] M. Piva, M. Iglesias, P. Bissio and A. Calvo, Experiments on Vortex Funnel Formation During Drainage, *Physica A* 329 (2003) 1-6.

[6] J. Lacapere, Focus on the CFD for the ARIANE 5 Launcher: Space Engineering Activities at Cryospace and Air Liquid, Fluent News, (2005). Available online at www.fluent.com/about/news/newsletters.

[7] M. J. Lewis and T. Rice, Design of a University Launch Vehicle System, *The 10th Applied Aerodynamics Conference*, Palo Alto, CA, AIAA 1992-2663.

[8] S. Chakroborty, J. R. Wertz and R. Conger, The Scorpius Expendable Launch Vehicle Family and Status of the Sprite Small Launch Vehicle, *The 1st Responsive Space Conference, Redondo Beach*, CA, AIAA 2003-9005.

[9] L. Virgil, J. Hutchinson and J. R. Olds , Estimation of Launch Vehicle Propellant Tank Structural Weight Using Simplified Beam Approximation, *The 40th AIAA/ASME/SAE/ASEE Joint Propulsion Conference and Exhibit*, Fort Lauderdale, Florida, USA, AIAA 2004-366.

[10] M. Mirshams, H. Karimi and H. Naseh, Launch Vehicle Conceptual Design (LVCD) Software based on multi-parameter optimization, *The 7th International. Aerospace Engineering Conference*, Tehran, Iran, Paper No. 281 (2008).

[11] A. Tewari, Atmospheric and Spaceflight Dynamics, Modeling and Simulation with Matlab and Simulink, Birkhauser, Boston, USA (2007).

[12] M. Turner, Rocket and Spacecraft Propulsion, Principles, Practice and New Developments, Springer, Chichester U.K. (2009).

[13] N. Yildirim and F. Kocabas, Prediction of Critical Submergence for an Intake Pipe, *Journal of Hydraulic Research*, 40 (4) (2002) 507-517.

[14] G. Echavez and E. McCann, An Experimental Study on the

Surface Vertical Vortex, *Experiments in Fluids*, 33 (3) (2002) 414-421.
[15] B. H. Lakshamana Gowda, P. J. Joshy and S. Swarnamani, Device to Suppress Vortexing during Draining from Cylindrical Tanks, *Journal of Spacecraft*, 33 (4) (1995) 598-600.
[16] G. Haller, on Objective Definition of a Vortex, *Journal of Fluid Mechanic*, 525 (2005) 1-26.
[17] T. Alrutz and M. Rutte, Investigation of Vortex Breakdown over a Pitching Delta Wing Applying the DLR TAU-Code with Full Automatic Grid Adaptation, *The 35th AIAA Fluid Dynamics Conference and Exhibit*, Toronto, Ontario, Canada, AIAA 2005-5162.
[18] A. J. Odgaard, Free Surface Air Core Vortex, *Journal of Hydraulic Engineering*, 112 (7) (1996) 610-620.
[19] C. Crowe, M. Sommerfield and Y. Tsuji, Multiphase Flows with Droplets and particles, (1998).
[20] H. K. Versteeg and W. Malalasekera, An Introduction to Computational Fluid Dynamics, *The Finite Volume Method*, 1st edition, Prentice Hall (1995).
[21] N. M. Beliaev, Calculation of Hydraulic Pneumatic System in a Rocket, Mashinostroenieh, Moscow, Russia (1983).
[22] W. E. Wiessel, Spaceflight Dynamics, McGraw-Hill, USA (1989).

M. Mahyari received his B.Sc. and M.Sc. in Mechanical Engineering from the K. N. Toosi University of Technology of Iran in 2006 and 2008, respectively. His research fields include experimental and computational fluid mechanics and heat transfer, modeling and simulation.

H. Karimi received his Ph.D. in Solid and Liquid Propellant Engine Design from the Moscow state Technical University in 1999. He joined the aerospace engineering department of K. N. Toosi University of Technology in 1999 where he is presently an associate professor and head of the propulsion group. He is also an organizing member of the Iranian Aerospace Society. His core research interests are gas dynamics, gas turbine, modeling, simulation and control of liquid and solid propellant engines.

H. Naseh received his M.Sc. in Aerospace Engineering from the K. N. Toosi University of Technology, Iran in 2007. His M.Sc. research involved conceptual design of aerospace vehicles. His research focuses on the space system engineering, optimal control, orbital mechanics and space propulsion engineering. He is a Ph.D. student at K. N. Toosi University, now.

M. Mirshams received his Ph.D. in Aerospace Engineering from the Moscow State Technical University in 1999. He has been a faculty member at K. N. Toosi University of Technology, Iran since 1999. His Ph.D. research involved space system engineering. His core research interests are launch vehicle and satellite system engineering, orbital mechanics, flight dynamics and simulation engineering.